Published in final edited form as:
Ultrasound Med Biol. 2007 July ; 33(7): 1140–1148. doi:10.1016/j.ultrasmedbio.2006.12.009.

The Natural Frequency of Nonlinear Oscillation of Ultrasound Contrast Agents in Microvessels

Shengping Qin and **Katherine W. Ferrara**
Department of Biomedical Engineering, University of California, Davis, CA, 95616, USA

Abstract

Ultrasound Contrast Agent (UCAs) are under intensive investigation for their applications in physiological and molecular imaging and drug delivery. Prediction of the natural frequency of the oscillation of UCAs in microvessels has drawn increasing attention. To our knowledge, the existing models to predict the natural frequency of oscillation of UCAs in microvessels all apply the linear approximation and treat the blood vessel wall as a rigid boundary. In the potential applications of ultrasound imaging drug and gene delivery, the compliance of small vessels may play an important role in the bubble's oscillation. The goal of this work is to provide a lumped-parameter model to study the natural frequency of nonlinear oscillation of UCAs in microvessels. Three types of the blood vessel conditions have been considered. i.e. rigid vessels, normal compliable vessels and vessels with increasing stiffness that could correspond to tumor vasculature. The corresponding bubble oscillation frequencies in the vessels with radius less than 100 μm are examined in detail. When a bubble with a radius of 4 μm is confined in a compliable vessel (inner radius 5 μm and length 100μm), the natural frequency of bubble oscillation increases by a factor of 1.7 as compared with a bubble in an unbounded field. The natural frequency of oscillation of a bubble in a compliable vessel increases with decreasing vessel size while decreasing with increasing values of vessel rigidity. This model suggests that contrast agent size, blood vessel size distribution and the type of vasculature should be comprehensively considered for choosing the transmitted frequency in ultrasound contrast imaging and drug delivery.

Keywords

drug delivery; ultrasound contrast agents; microbubble oscillation; nonlinear oscillation; blood vessels; natural frequency; vessel rigidity; compliable vessels

1. Introduction

Ultrasound contrast agents (UCAs) are gas bubbles with a diameter from 1 to 5 μm and are filled with air or a high molecular weight gas such as sulfur hexafluoride or perfluorocarbon. Due to the great difference in density and compressibility of microbubbles compared with plasma and their resonance frequencies in the range of diagnostic ultrasound frequencies, a small volume of agents produces a large echo. UCAs enhance the visualization of the blood pool by as much as 40 dB and thus allow the detection of vessels as small as capillaries (Bloch

Corresponding author, Shengping Qin, Department of Biomedical Engineering, University of California, Davis, One Shields Avenue, CA, 95616, USA, Phone: (530)754-9450, Fax: (530)754-5739, E-mail:spqin@ucdavis.edu.

et al. 2004; Broumas et al. 2005). The nature of the oscillation of microbubbles within blood vessels in response to transmitted ultrasound (US) waves is nonlinear and thus the echoes from the UCAs can be distinguished from those of other strong scatters. Subharmonic imaging strategies use the nonlinear components of the scattered echoes from microbubbles to provide a high contrast agent-to-tissue ratio, as tissue does not generate measurable subharmonic components at diagnostic intensity levels (Krishna et al. 1999; Bhagavatheeshwaran et al. 2004). In typical subharmonic imaging, the UCAs are interrogated at approximately twice their resonant frequency and the resonant-frequency echoes are detected. Therefore, the prediction of a bubble's natural frequency within small blood vessels plays an important role in constructing a subharmonic imaging algorithm.

In therapy, numerous investigators have indicated that ultrasound microbubbles may be the promising drug delivery vehicles (Lindner and Kaul 2001; Chomas et al. 2001; Riess 2003; Stride and Saffari 2003; Unger et al. 2004; Bekeredjian et al. 2005; Klibanov 2006; Borden et al. 2006; Chappell and Price 2006). As drug delivery agents, microbubbles are bound to or encapsulated with a drug. When the microbubbles circulate in bloodstream and arrive at the target site, a series of long, low amplitude ultrasound pulses are employed to deflect the bubbles toward the blood vessel wall. If the bubbles are driven near the resonance frequency, they can experience a large net ultrasound radiation force (USRF) in the direction of ultrasound wave propagation and thus a large displacement (Lum et al. 2006). Bubble adhesion efficiency can thus be improved by 20-fold by localizing bubbles along a vessel wall with USRF (Zhao et al. 2000; Rychak et al. 2005). When the bubbles are attached to the vessel wall, the fragmenting ultrasound pulses are administrated to rupture the bubbles and release drugs at the target site. In order to rupture the bubbles near the target vessel wall, the fragmenting ultrasound frequency is typically lower than bubble's resonance frequency. This local drug delivery technique can reduce the systemic toxicity and also improve the efficacy. In both contrast-enhanced ultrasound imaging and drug delivery with bubbles, the target site is usually small blood vessels such as arterioles, capillaries and venules whose typical diameter ranges from 8 μm to 30 μm. After insonation, the bubble oscillates in small vessels (Caskey et al. 2006a; Caskey et al. 2006b). Therefore, the consistent and accurate prediction of UCA natural frequency in microvessel may play a significant role in these medical applications.

The natural frequency of gas bubbles has primarily been studied in unbounded liquids (Plesset and Prosperetti 1977; Prosperetti et al. 1988; Feng and Leal 1997; Khismatullin 2004; Khabeev 2006). However, due to the nonlinearity of bubble oscillation in small blood vessels the natural frequency of a bubble strongly depends on the boundaries in the vicinity of the bubbles and also the bubble size (Oguz and Prosperetti 1998; Krasovitski and Kimmel 2001; Broumas et al. 2005). Oguz and Prosperetti (Oguz and Prosperetti 1998) and Sassaroli and Hynynen (Sassaroli and Hynynen 2004; Sassaroli and Hynynen 2005) pioneered the investigation of the effect of a rigid tube boundary on gas bubble natural frequency using a linear approximation method. They predicted that the natural frequency of a bubble in a rigid tube decreases with decreasing tube size and with increasing bubble radius. However, because of the limitation of linear perturbation method, different approximation strategies must be employed for each range of the ratio of microbubble and tube radius. In addition, the rigid tube assumption results in a dependency of the bubble natural frequency on both the tube length and the relative position of the bubble in the tube. Because the liquid is usually assumed to be incompressible, bubble oscillation would be nonexistent if the tube length were infinite. However, in our *ex vivo* experimental data (not shown), we consistently found that microbubbles oscillate periodically in relatively long rat cecum capillaries (Caskey et al. 2006b).

The rigidity of capillaries may be derived primarily from the studies in (Baez S et al. 1960; Lamport and Baez 1962), who reported that capillary diameter in the rat meso-appendix remained constant over a very wide range of pressure. However, they stated that the accuracy

of their dimensional measurement was 2.75 μm and therefore was insufficient to record diameter changes of the size expected to occur in capillaries due to dispensability. Since the 1980s, some evidence has indicated that capillaries are distensible (Swayne and Smaje 1984; Smaje and Swayne 1984; Baldwin and Gore 1989; Swayne et al. 1989; Swayne and Smaje 1989; Bosman et al. 1995; Neal and Michel 1996; Lenz J.F. 1998; Kindig and Poole 1999; Kassab et al. 1999; Neal and Michel 2000). In our current *in vivo* experiments, we observed that the intravenously injected dextran can extravasate through the microvessel wall as a result of ultrasound (1.3MPa 1MHz) with UCAs(Stieger et al. 2006). The distensibility of a microvessel may play a vital role in the opening of microvascular endothelium in ultrasound-enhanced drug delivery (Neal and Michel 1996). The goal of this work is to provide a lumped-parameter model to study the natural frequency of nonlinear oscillation of UCAs in microvessels for potential applications in ultrasound contrast imaging and drug delivery. To the best of our knowledge, there are no theoretical or experimental data describing the natural frequency of UCAs in compliable vessels. The paper is organized as follows: in Section 2, the theoretical method is discussed along with the anatomy of capillary blood vessels and the factors affecting the compliance of vessels. In Section 3, numerical results for the natural frequency will be analyzed as a function of the tube size and bubble size as well as the stage of tumor development. Sections 4 and 5 provide discussion and conclusions.

2. Method

In order to numerically study the natural frequency of UCAs within microvessels, an initially spherical microbubble lying at the center of a blood-filled circular cylindrical vessel is expanded slightly from its equilibrium diameter and then released. The succeeding oscillation of the bubble is studied, Figure 1(a). The basic governing equations, boundary conditions and numerical strategy developed in (Qin and Ferrara 2006) will be employed in this work, while distinct characteristics are described in this section.

Blood is simplified as an incompressible viscous Newtonian fluid with an effective viscosity two times viscosity of water (Sassaroli and Hynynen 2004). The undisturbed local physiological pressure is used as the pressure boundary condition at the ends of the vessel (Rubinow and Keller 1972). The undisturbed intraluminal pressure in the micro-vessel is chosen to 105.37 kPa, which is the average of the representative pressure in arterioles (108.6kPa), capillaries (104.6kPa) and venules (102.9kPa). Because the UCA shell thickness is usually between 10 nm to 520 nm, it can be treated as a gas bubble which obeys the polytropic law:

$$p_g = p_{ge}\left(\frac{V_e}{V}\right)^{\kappa}. \tag{1}$$

The polytropic index κ takes the value between 1 (isothermal behavior) and γ_g, ratio of constant-pressure to constant-volume specific heats for the gas (adiabatic behavior). In small amplitude oscillation, the isothermal behavior prevails for a small gas bubble and low frequency (Chapman and Plesset 1971). Thus in this work, $\kappa = 1$, which is different from $\kappa = 1.4$ for a large deformation study (Qin and Ferrara 2006). At the air-blood interface, continuity of stress and velocity is employed in the normal direction.

A capillary vessel wall is composed of a single layer of endothelial cells of about 1 μm in thickness, which is enveloped by a basement membrane. As many investigators have noted, the compliance and the deformation of the capillaries depend on the thickness of the tissue surrounding the blood vessel and on the degree to which the surrounding tissue is stressed (Fung et al. 1966; Sassaroli and Hynynen 2004). The crucial question is whether the

surrounding medium is a fluid or an elastic solid. An elastic solid is capable of transmitting shear stress in a static conduction but a fluid cannot do so. The static torsion test revealed that the connective tissue matrix is able to resist shear very well. Therefore in theoretical analysis, the capillary is usually modeled as a tunnel in an elastic medium (the connective tissue gel) (Fung et al. 1966), as illustrated in Figure 1 (b). In order to study tissue compliance for different tissue matrices, a sophisticated biomechanics model is needed, such as the elastic model based on continuum mechanics proposed by (Fung et al. 1966). In this paper, we used the following lumped-parameter model to include the effect of perivascular reactive radial stress and the inertial effect of vessels and surrounding gel to examine the bubble's natural frequency in compliable vessels(Misra and Singh 1983; Humphrey and Na 2002; Qin and Ferrara 2006):

$$\rho_c h_c \ddot{r}_i + \rho_t h_t \ddot{r}_i = p_i - p_a - \sigma_0 \frac{e^{\beta(\delta-1)} - 1}{\gamma\delta^2 - 1/2} - Y\xi(1-\nu^2)E_\theta(R_a,t), \tag{2}$$

where the cap double dot means the second derivative with respect to time t; σ_0 and β are two material-dependent stress-strain parameters; $\gamma = R_m / H$ and $\delta = r_m / R_m$. The notation of the symbols is listed in table 1. The first term on the left-hand side of equation (2) is the inertial stress of the blood vessel; the second term on the left-hand side of equation (2) is the effective inertial stress of surrounding tissue. The term $p_i - p_a$ with $p_a = p_0$ is the transmural pressure through the vessel wall. The third term on the right-hand side of equation (2) is the blood vessel's static response relationship. The last term on the right-hand side of equation (2) is the perivascular reactive radial stress. $E_\theta(R_a, t)$ is approximated by $\frac{1}{2}\left(\delta^2 - 1\right)$, $\xi = 0.1$ and $\nu = 0.5$ (Misra and Singh 1983).

Blood vessel compliance and that of the surrounding tissue are thought to vary across tissue types (fat, muscle, brain) and decrease as a tumor develops(Jain 1988; Jang et al. 2003; Sarntinoranont et al. 2003). The relationship among the mechanical properties of the vasculature, tumor volume and vessel wall thickness have not been thoroughly characterized. As a first effort to study the characteristics of the bubble natural frequency in compliable vessels as a tumor develops, we use the following quantitative functions to approximate the changes of the vasculature elasticity and the effective dynamic thickness of the surrounding tissue as the tumor develops(Belardinelli and Cavalcanti 1992; Qin and Ferrara 2006).

$$\begin{aligned} \sigma_0 &= 4101(2k+1)Pa \\ \beta &= 15.35(k+1) \\ Y &= 8\times 10^5(2k+1)Pa \\ h_t &= R_a(\xi + e^k - 1) \end{aligned} \tag{3}$$

When $k = 0$, the corresponding parameters are $\sigma_0 = 4101Pa$, $\beta = 15.35$, $Y = 8\times10^5\ Pa$ and $h_t = 0.1R_a$, which correspond to normal compliable vasculature for which the parameters were obtained previously in *ex vivo* experiments for exteriorized mesentery (Swayne G.T.G 1984). When the values of k in equation (3) are extremely large, a compliable vessel will reduce to a rigid wall, the coupling equation (2) will be diminished and replaced by the traditional non-slip condition ($v_r = 0, v_z = 0$). Unless stated otherwise, the parameter symbols and corresponding values used in computation are listed in table 1.

3. Results

If the microvessel radius is significantly larger than that of the bubble, the oscillation of the bubble in the vessel should asymptotically approach to that of the bubble in the unbounded field. We first compared the results of the present model with those obtained by the independent method, Rayleigh-Plesset equation, to demonstrate its accuracy. Figure 2 shows that they are in excellent agreement.

3.1 The natural frequency of oscillation of a bubble within a rigid microvessel

The effect of the rigid vessel boundary on the natural frequency of oscillation of a bubble was first examined. Figures 3 (a) and (b) show that the natural frequency of a bubble in a small rigid vessel is substantially decreased. The natural frequency of a bubble in the corresponding unbounded field is the upper limit of that in the rigid vessel. The free natural frequency of oscillation of a bubble with a_0 = 1 μm, 2 μm, 3 μm and 4 μm in the unbounded field is f_0 = 3.65 MHz, 1.61 MHz, 1.01 MHz, 0.74 MHz, respectively. The frequency decreases to 0.74 MHz (0.20 f_0), 0.22 MHz (0.14 f_0), 0.11 MHz (0.11 f_0), and 0.062 MHz (0.08 f_0), respectively, when the bubble is confined at the center of a rigid vessel with $R_0 = 5\mu m$, $L = 500\mu m$. For a bubble with the same initial radius, when the vessel size approaches the bubble size, the effect of the rigid vessel is enhanced. This is represented by the increasing slope with decreasing vessel radius in Figure 3 (a). Also, in small vessels ($R_0 \leq 20\mu m$) (the typical vessel size where the UCA-delivered drugs would be released), the change in frequency with vessel size ($\delta f / \delta R$) is larger for a smaller bubble. For example, in a 5 μm radius vessel, $\delta f / \delta R$ =0.15 MHz/μm for a bubble radius of 1 μm and $\delta f / \delta R$ =0.018MHz/μm for a bubble radius of 4 μm (Figure 3 (a)).

In ultrasound-assisted drug delivery, drug extravasation through the blood vessel wall is usually observed in small blood vessels ($R_0 \leq 20\mu m$) *in vivo* experiments(Stieger et al. 2006). In Figure 4(a) and (b), we studied the natural frequency of UCAs as a function of bubble radius in representative vessels (R = 5, 10, $20\mu m$). For the same size of the vessel, the bubble natural frequencies decrease with increasing the bubble size, which is consistent with the trend in unbounded field (Figures 4 (a)). For example, f = 0.74 MHz, 2.46MHz for the a_0 = 1 bubble in R_0 = 5, $20\mu m$ vessels, respectively, decrease to 0.062 MHz and 0.31 MHz with the bubble radius increasing to 4μm.

3.2 The natural frequency of oscillation of a bubble within a compliable microvessel (k=0)

Figures 5 (a) and (b) show that the natural frequency of oscillation of a bubble in a compliable vessel increases with decreasing vessel size. The natural frequency of a bubble in the unbounded field is the lower limit of the bubble natural frequency in the compliable vessel. For example, when the bubble is confined in compliable vessels with $R_0 = 5\mu m$ and L = $100\mu m$, the natural frequency of a bubble of radius 1 μm, 2 μm, 3 μm and 4 μm increases to 3.92 MHz (1.07 f_0), 1.93 MHz (1.20 f_0), 1.41 MHz (1.38 f_0), and 1.26 MHz (1.70 f_0), respectively. For a bubble with the same initial radius, when the vessel size approaches the bubble size, the effect of the compliable vessel is enhanced. This is represented by the increasing slope (absolute value) with decreasing vessel radius in Figure 5 (a). In small vessels ($R_0 \leq 20\mu m$) the compliable vessel boundary has a noticeable effect on the bubble oscillation frequency. Beyond this range the natural frequency can be approximated by the Rayleigh-Plesset equation. For example, in a vessel with an initial radius of 20 μm, the natural frequency of a bubble with $a_0 = 1\mu m$ is approximately equal to $f_0 = 3.65MHz$ (Figure 5(a)). For small vessels ($R_0 \leq 20\mu m$), the change of the frequency with vessel size ($|\delta f / \delta R|$) is larger for larger bubbles, and thus the effect is different from that in rigid vessels. In a vessel with an initial radius of 5μm, $|\delta f / \delta R|$=0.49MHz/μm for the a_0 = 1 μm bubble and $|\delta f / \delta R|$=0.10MHz/μm for the a_0 = 4μm bubble (Figure 5 (a)).

The natural frequency of the typical size of UCAs as a function of bubble radius in representative compliable vessels (R = 5, 10, 20μm) was plotted in Figure 6(a) and (b). For the same radius vessel, the bubble natural frequency decreases with increasing bubble radius, which is consistent with the trend in the unbounded field (Figures 6 (a)) and in the rigid vessel (Figures 4 (a)). For example with a_0 = 1, f = 3.92 MHz and 3.65 MHz in compliable vessels with an initial radius of 5 and 20 μm, respectively, and decreases to 1.26MHz and 0.81MHz when the bubble radius increases to 4 μm. For a vessel with the same initial inner radius, the dimensionless natural frequency increases with increasing bubble radius (Figure 6 (b)), which is different from the trend in the rigid vessel (Figure 4 (b)). Thus, the compliable vessel boundary has a stronger effect in increasing frequency for a larger bubble radius.

3.3 The natural frequency of oscillation of a bubble within a compliable microvessel with increasing k

Equation (3) was employed to study the natural frequency of oscillation of a bubble in a microvessel as a tumor develops. Figures 7 (a) and (b) show that the natural frequency of a bubble with initial radius of 4 μm in a blood vessel of R_0 = 5 μm decreases with increasing values of k. The bubble frequency approaches that in a rigid vessel as the stiffness increases, which is significantly lower than that in the unbounded field and in the normal tissue. In a normal vessel the bubble natural frequency is $f_0{}'$=1.26MHz and it decreases to 0.74MHz (0.59 $f_0{}'$) at k=1.07, which equals that in the unbounded field. When a tumor develops further and stiffness increases, the frequency further decreases to 0.062 MHz (0.048 $f_0{}'$).

4. Discussion

The goal of this work is to provide a numerical method to study the nonlinear oscillation frequency of a bubble confined in microvessels. The linear approximation method has been used previously to predict bubble natural frequency in a rigid vessel (Oguz and Prosperetti 1998; Sassaroli and Hynynen 2004; Sassaroli and Hynynen 2005). In order to compare the results obtained by present model with those from the linear approximation method (Sassaroli and Hynynen 2005), the parameters such as blood density ρ, blood effective viscosity η, the initial intraluminal pressure p_{i0}, the blood vessel length L and bubble initial radius a_0 were chosen to be the same as those in the literature (Sassaroli and Hynynen 2005). The present results (Figures 3) are consistent with those in Figure 5 in (Sassaroli and Hynynen 2005). For example, the predicted natural frequency of a bubble with initial radius of 1 μm in a rigid vessel of radius 20 μm are 2.50MHz for both methods, Figure 5 (Sassaroli and Hynynen 2005) and Figure 3 in this work. However, when the ratio of bubble radius over blood vessel radius a_0 / R_0 increases, there is a discrepancy between the results predicted by the linear approximation and the present nonlinear method due to the approximations included in the linear method (see details in the introduction and discussion sections in (Sassaroli and Hynynen 2005)).

Because of the blood incompressibility assumption, the bubble's natural frequency in a rigid vessel is a function of the bubble's location relative to the vessel ends, as studied in (Oguz and Prosperetti 1998; Sassaroli and Hynynen 2004; Sassaroli and Hynynen 2005). Our current *ex vivo* observation that the microbubble and the blood vessel wall can periodically oscillate with a relatively low velocity as compared to the wave speed in the blood in the relatively long rat cecum capillaries indicates that the compliance of the blood vessel may play a vital role in the bubble's oscillation (Caskey et al. 2006b). If the vessel is distensible, the volume change of the bubble is compensated by the deformation of the blood vessel wall and only the nearby region of the vessel is affected by bubble's oscillation (Qin et al. 2006). The natural frequency of a bubble within a compliable vessel is therefore less dependent on the bubble's location relative to the vessel ends. In this work, we examined this characteristic and found that if the

length of the vessel of interest is longer 100 μm, increasing the vessel length does not change the bubble's natural frequency.

Vascular compliance across a wide range of vessel sizes and tissue types has not been thoroughly characterized. The parameters used to study the natural frequency of a bubble in normal microvessels studied in this work were determined for the exteriorized frog mesenteric capillary, which may not represent the general characteristic for the microvessels. In computation, $\xi = 0.1$ and $k = 0$ in equation (3) indicate that the surrounding tissue thickness is only 0.1 of the outer radius of the vessel (Misra and Singh 1983). The results in this work thus may present the natural frequency of a bubble in an isolated small vessel, which is the *ex vivo* experimental environment for intravital microscopy and window chamber models often used in model systems.

The development of a tumor can increase the rigidity of the vasculature and interstitial tissue, however changes in the compliance of tumor vessels and surrounding tissue are currently not well characterized. In equation (3), we hypothesize that rigidity of the vasculature and interstitial tissue and the thickness of the connective tissue grow as the tumor develops. The correlation between volume growth and rigidity need to be determined for different vasculature morphologies and for tumors. If the volume growth is slower than the proposed rate, we found that the bubble natural frequency could increase during the tumor development period, which can be illustrated by an increase in the natural frequency of a spring-mass system as the spring elastic modulus increases. But when the tumor develops to several cm^3, the vessel wall can be rigid and the natural frequency could decrease to the predicted values (Figure 7). An accurate biomechanical model for tumor vessels and tissue and corresponding *in vivo* experimental data are needed for improved imaging and drug delivery in tumors.

5. Conclusion

In this work, we proposed a lumped-parameter model to study the natural frequency of nonlinear oscillation of microbubbles in microvessels. Three models for blood vessel compliance have been considered. i.e. a rigid vessel, normal compliable vessel and a stiff vessel which may correspond to the vasculature of a developing tumor. The perivascular reactive stress of the surrounding tissue and the inertial effect of the microvessel and surrounding tissue have been hypothesized. Numerical results demonstrate that the natural frequency of a bubble in a rigid vessel is substantially decreased as compared to that in unbounded field. The natural frequency of a bubble in a rigid vessel further decreases with a decrease in the confining vessel size. For the same vessel size, the bubble natural frequency decreases with increasing bubble size, which is consistent with the trend in an unbounded field. Within a compliable vessel, modeling an exteriorized frog mesenteric capillary, the natural frequency of oscillation of a bubble increases with decreasing vessel size, and with a constant vessel diameter the bubble dimensionless natural frequency increases with increasing bubble size. The natural frequency of a bubble in the unbounded field is the lower limit of the bubble natural frequency in the compliable vessel and the upper limit of that in a rigid vessel. Under the conditions studied, the natural frequency of bubble oscillation decreases as a tumor develops.

Acknowledgements

The support of NIH CA 76062 and CA 103828 are gratefully appreciated.

References

Baez, S.; Lamport, H.; Baez, A. Pressure Effects in Living Microscopic Vessels. In: Copley, AL.; Stainsky, G., editors. Flow Properties of Blood. London: Pergamon Press, Inc; 1960.

Baldwin AL, Gore RW. Simultaneous Measurement of Capillary Distensibility and Hydraulic Conductance. Microvascular Research 1989;38(1):1–22. [PubMed: 2788240]

Bekeredjian R, Grayburn PA, Shohet RV. Use of ultrasound contrast agents for gene or drug delivery in cardiovascular medicine. Journal of the American College of Cardiology 2005;45(3):329–335. [PubMed: 15680708]

Belardinelli E, Cavalcanti S. Theoretical-Analysis of Pressure Pulse-Propagation in Arterial Vessels. Journal of Biomechanics 1992;25(11):1337–1349. [PubMed: 1400535]

Bhagavatheeshwaran G, Shi WT, Forsberg F, Shankar PM. Subharmonic signal generation from contrast agents in simulated neovessels. Ultrasound in Medicine and Biology 2004;30(2):199–203. [PubMed: 14998672]

Bloch SH, Dayton PA, Ferrara KW. Targeted imaging using ultrasound contrast agents. Ieee Engineering in Medicine and Biology Magazine 2004;23(5):18–29. [PubMed: 15565796]

Borden MA, Martinez GV, Ricker J, Tsvetkova N, Longo M, Gillies RJ, Dayton PA, Ferrara KW. Lateral phase separation in lipid-coated microbubbles. Langmuir 2006;22(9):4291–4297. [PubMed: 16618177]

Bosman J, Tangelder GJ, Egbrink MGAO, Reneman RS, Slaaf DW. Capillary Diameter Changes During Low Perfusion-Pressure and Reactive Hyperemia in Rabbit Skeletal-Muscle. American Journal of Physiology-Heart and Circulatory Physiology 1995;38(3):H1048–H1055.

Broumas AR, Pollard RE, Bloch SH, Wisner ER, Griffey S, Ferrara KW. Contrast-enhanced computed tomography and ultrasound for the evaluation of tumor blood flow. Investigative Radiology 2005;40 (3):134–147. [PubMed: 15714088]

Caskey CF, Kruse DE, Dayton PA, Kitano TK, Ferrara KW. Microbubble oscillation in tubes with diameters of 12, 25, and 195 microns. Applied Physics Letters 2006a;88(3)

Caskey CF, Stieger SM, Dayton PA, Ferrara KW. High-Speed Imaging with Copper Vapor Laser Increases Contrast. 2006 IEEE Ultrasonics Symposium. 2006b

Chapman RB, Plesset MS. Thermal Effects in Free Oscillation of Gas Bubbles. Journal of Basic Engineering 1971;93(3):373–376.

Chappell JC, Price RJ. Targeted therapeutic applications of acoustically active microspheres in the microcirculation. Microcirculation 2006;13(1):57–70. [PubMed: 16393947]

Chomas JE, Dayton P, Allen J, Morgan K, Ferrara KW. Mechanisms of contrast agent destruction. IEEE Transactions on Ultrasonics Ferroelectrics and Frequency Control 2001;48(1):232–248.

Feng ZC, Leal LG. Nonlinear bubble dynamics. Annual Review of Fluid Mechanics 1997;29:201–243.

Fung YC, Zweifach BW, INTAGLIE M. Elastic Environment of Capillary Bed. Circulation Research 1966;19(2):441–461. [PubMed: 5914856]

Humphrey JD, Na S. Elastodynamics and arterial wall stress. Annals of Biomedical Engineering 2002;30 (4):509–523. [PubMed: 12086002]

Jain RK. Determinants of Tumor Blood-Flow - A Review. Cancer Research 1988;48(10):2641–2658. [PubMed: 3282647]

Jang SH, Wientjes MG, Lu D, Au JLS. Drug delivery and transport to solid tumors. Pharmaceutical Research 2003;20(9):1337–1350. [PubMed: 14567626]

Kassab GS, Le KN, Fung YCB. A hemodynamic analysis of coronary capillary blood flow based on anatomic and distensibility data. American Journal of Physiology-Heart and Circulatory Physiology 1999;277(6):H2158–H2166.

Khabeev NS. Resonance properties of soluble gas bubbles. International Journal of Heat and Mass Transfer 2006;49(56):1022–1026.

Khismatullin DB. Resonance frequency of microbubbles: Effect of viscosity. Journal of the Acoustical Society of America 2004;116(3):1463–1473. [PubMed: 15478411]

Kindig CA, Poole DC. Effects of skeletal muscle sarcomere length on in vivo capillary distensibility. Microvascular Research 1999;57(2):144–152. [PubMed: 10049662]

Klibanov AL. Microbubble contrast agents - Targeted ultrasound imaging and ultrasound-assisted drug-delivery applications. Investigative Radiology 2006;41(3):354–362. [PubMed: 16481920]

Krasovitski B, Kimmel E. Gas bubble pulsation in a semiconfined space subjected to ultrasound. Journal of the Acoustical Society of America 2001;109(3):891–898. [PubMed: 11303943]

Krishna PD, Shankar PM, Newhouse VL. Subharmonic generation from ultrasonic contrast agents. Physics in Medicine and Biology 1999;44(3):681–694. [PubMed: 10211802]

Lamport H, Baez S. Physical Properties of Small Arterial Vessels. Physiological Reviews 1962;42:328–352. [PubMed: 14461855]

Lenz, JF. Micromechanics of Capillaries: Reflectance Confocal Microscopy of Single Microvessels in vivo. University of California; Davis: 1998. Ref Type: Thesis/Dissertation

Lindner JR, Kaul S. Delivery of drugs with ultrasound. Echocardiography-A Journal of Cardiovascular Ultrasound and Allied Techniques 2001;18(4):329–337.

Lum AFH, Borden MA, Dayton PA, Kruse DE, Simon SI, Ferrara KW. Ultrasound radiation force enables targeted deposition of model drug carriers loaded on microbubbles. Journal of Controlled Release 2006;111(12):128–134. [PubMed: 16380187]

Misra JC, Singh SI. A Large Deformation Analysis for Aortic Walls Under A Physiological Loading. International Journal of Engineering Science 1983;21(10):1193–1202.

Neal CR, Michel CC. Openings in frog microvascular endothelium induced by high intravascular pressures. Journal of Physiology-London 1996;492(1):39–52.

Neal CR, Michel C. Effects of temperature on the wall strength and compliance of frog mesenteric microvessels. Journal of Physiology-London 2000;526(3):613–622.

Oguz HN, Prosperetti A. The natural frequency of oscillation of gas bubbles in tubes. Journal of the Acoustical Society of America 1998;103(6):3301–3308.

Plesset MS, Prosperetti A. Bubble Dynamics and Cavitation. Annual Review of Fluid Mechanics 1977;9:145–185.

Prosperetti A, Crum LA, Commander KW. Nonlinear Bubble Dynamics. Journal of the Acoustical Society of America 1988;83(2):502–514.

Qin SP, Ferrara KW. Acoustic response of compliable microvessels containing ultrasound contrast agents. Physics in Medicine and Biology 2006;51(20):5065–5088. [PubMed: 17019026]

Qin SP, Hu YT, Jiang Q. Oscillatory Interaction between Bubbles and Confining Micro-Vessels and Its Implications on Clinical Vascular Injuries of Shock-Wave Lithotripsy. IEEE Transactions on Ultrasonics Ferroelectrics and Frequency Control 2006;53(7):1322–1329.

Riess JG. Fluorocarbon-based injectable gaseous microbubbles for diagnosis and therapy. Current Opinion in Colloid & Interface Science 2003;8(3):259–266.

Rubinow SI, Keller JB. Flow of A Viscous-Fluid Through An Elastic Tube with Applications to Blood-Flow. Journal of Theoretical Biology 1972;35(2):299–313. [PubMed: 5039296]

Rychak JJ, Klibanov AL, Hossack JA. Acoustic radiation force enhances targeted delivery of ultrasound contrast microbubbles: In vitro verification. IEEE Transactions on Ultrasonics Ferroelectrics and Frequency Control 2005;52(3):421–433.

Sarntinoranont M, Rooney F, Ferrari M. Interstitial stress and fluid pressure within a growing tumor. Annals of Biomedical Engineering 2003;31(3):327–335. [PubMed: 12680730]

Sassaroli E, Hynynen K. Forced linear oscillation's of microbubbles in blood capillaries. Journal of the Acoustical Society of America 2004;115(6):3235–3243. [PubMed: 15237848]

Sassaroli E, Hynynen K. Resonance frequency of microbubbles in small blood vessels: a numerical study. Physics in Medicine and Biology 2005;50(22):5293–5305. [PubMed: 16264254]

Smaje LH, Swayne GTG. The Effects of Compliance on Measurement of Hydraulic Conductivity in Microvessels. Biorheology 1984;21(12):171–179. [PubMed: 6466786]

Stieger SM, Charles CF, Adamson RH, Qin SP, Curry F-RE, Wisner ER, Ferrara KW. Enhancement of vascular permeability with low frequency contrast ultrasound using the chorioallantoic membrane model. Radiology. 2006in press

Stride E, Saffari N. On the destruction of microbubble ultrasound contrast agents. Ultrasound in Medicine and Biology 2003;29(4):563–573. [PubMed: 12749926]

Swayne, GTG. The Effect of Histamine on the Permeability of Rat Mesenteric Venules. Vol. 147. University of London; 1984. Ref Type: Thesis/Dissertation

Swayne GTG, Smaje LH. The Distensibility of Microvessels of the Frog and Rat Mesentery. International Journal of Microcirculation-Clinical and Experimental 1984;3(34):355.

Swayne GTG, Smaje LH. Dynamic Compliance of Single Perfused Frog Mesenteric Capillaries and Rat Venules - A Filtration Coefficient Correction. International Journal of Microcirculation-Clinical and Experimental 1989;8(1):43–52.

Swayne GTG, Smaje LH, Bergel DH. Distensibility of Single Capillaries and Venules in the Rat and Frog Mesentery. International Journal of Microcirculation-Clinical and Experimental 1989;8(1):25–42.

Unger EC, Porter T, Culp W, Labell R, Matsunaga T, Zutshi R. Therapeutic applications of lipid-coated microbubbles. Advanced Drug Delivery Reviews 2004;56(9):1291–1314. [PubMed: 15109770]

Zhao S, Borden M, Bloch SH, Kruse D, Ferrara KW, Dayton PA. Radiation-force assisted targeting facilitates ultrasonic molecular imaging. Molecular Imaging 2000;3(3):135–148. [PubMed: 15530249]

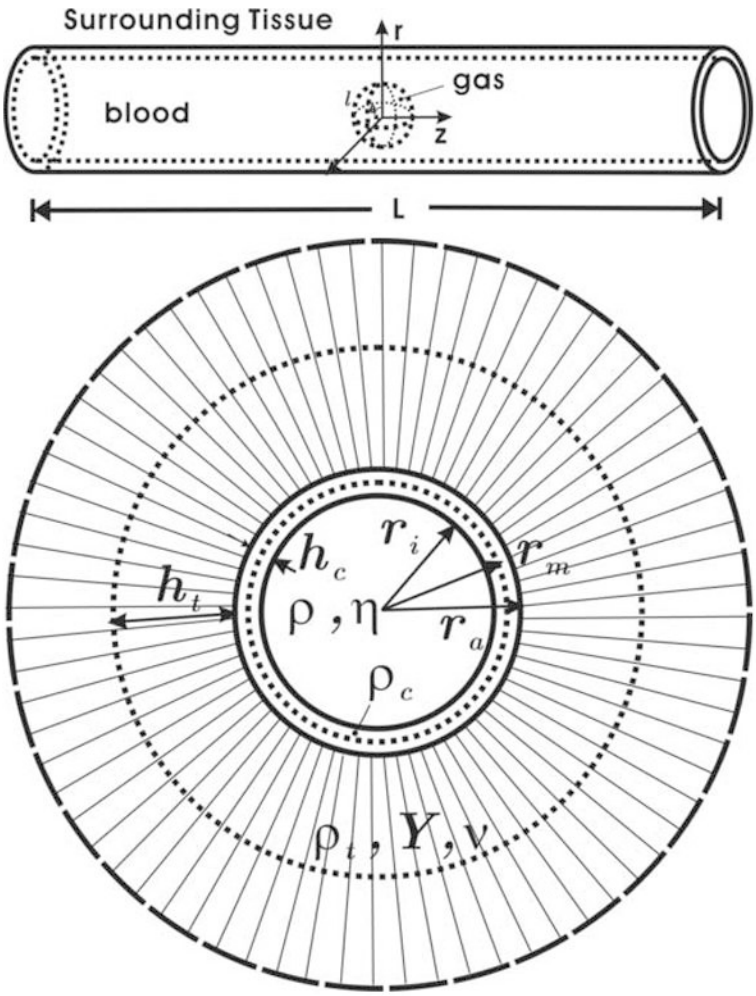

Figure 1.
An illustration of a microbubble confined in a microvessel: (a) the bubble is initially spherical lying at the center of the blood-filled cylindrical blood vessel; (b) a simplified schema of the blood vessel embedded in a gel. Symbols are defined in the table 1.

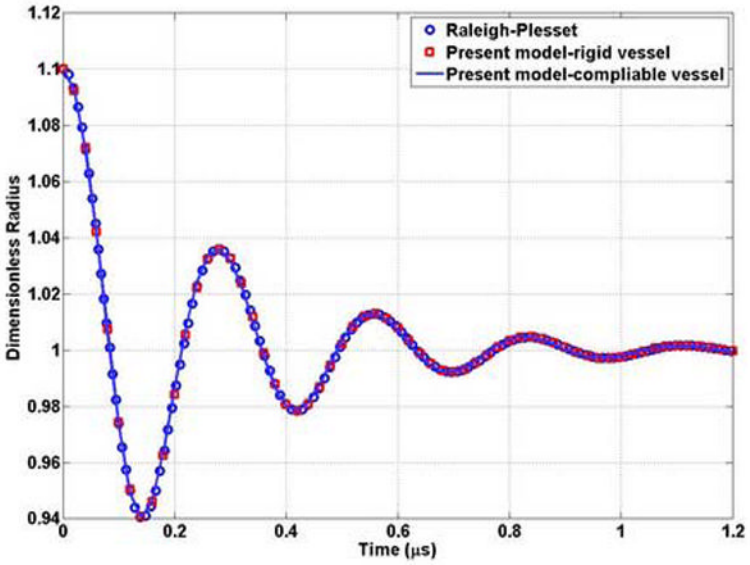

Figure 2.

Comparison the results of the present model with those obtained by an independent method, the Rayleigh-Plesset equation. A bubble with $a_0 = 1\mu m$ is expanded to 1.1μm position and released. The rigid vessel for the present model has length and radius of 500 and 150 μm, respectively. The compliable vessel ($k=0$) for the present model has length and radius of 500 and 50 μm, respectively. In both cases, the bubble is located in the center of the vessel.

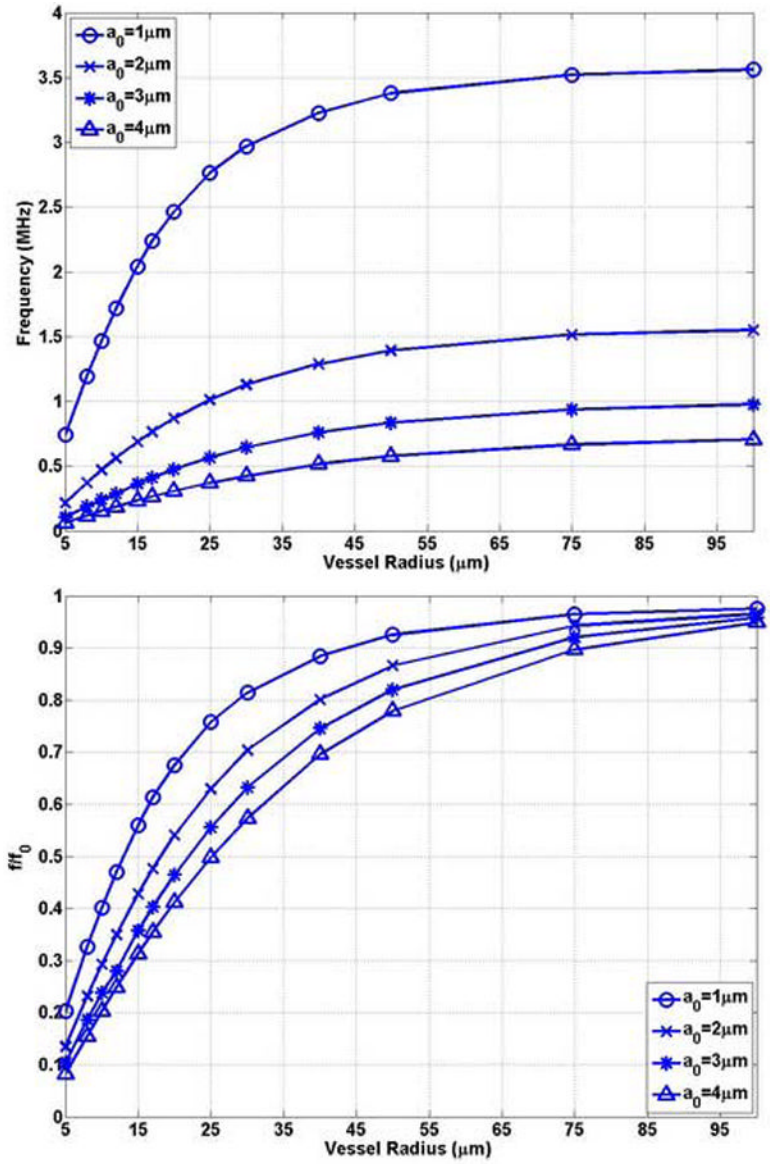

Figure 3.

The bubble natural frequency as a function of the vessel inner radius for bubbles lying in the center of rigid vessels with $L = 500\mu m$: (a) dimensional natural frequency; (b) dimensionless natural frequency, which is the normalized natural frequency of a bubble in the corresponding unbounded field predicted by the Rayleigh-Plesset equation $f_0=\frac{1}{2\pi}\sqrt{\frac{3\kappa(p_0+2\sigma/a_0)}{\rho a_0^2}-\frac{2\sigma}{\rho a_0^3}}$.

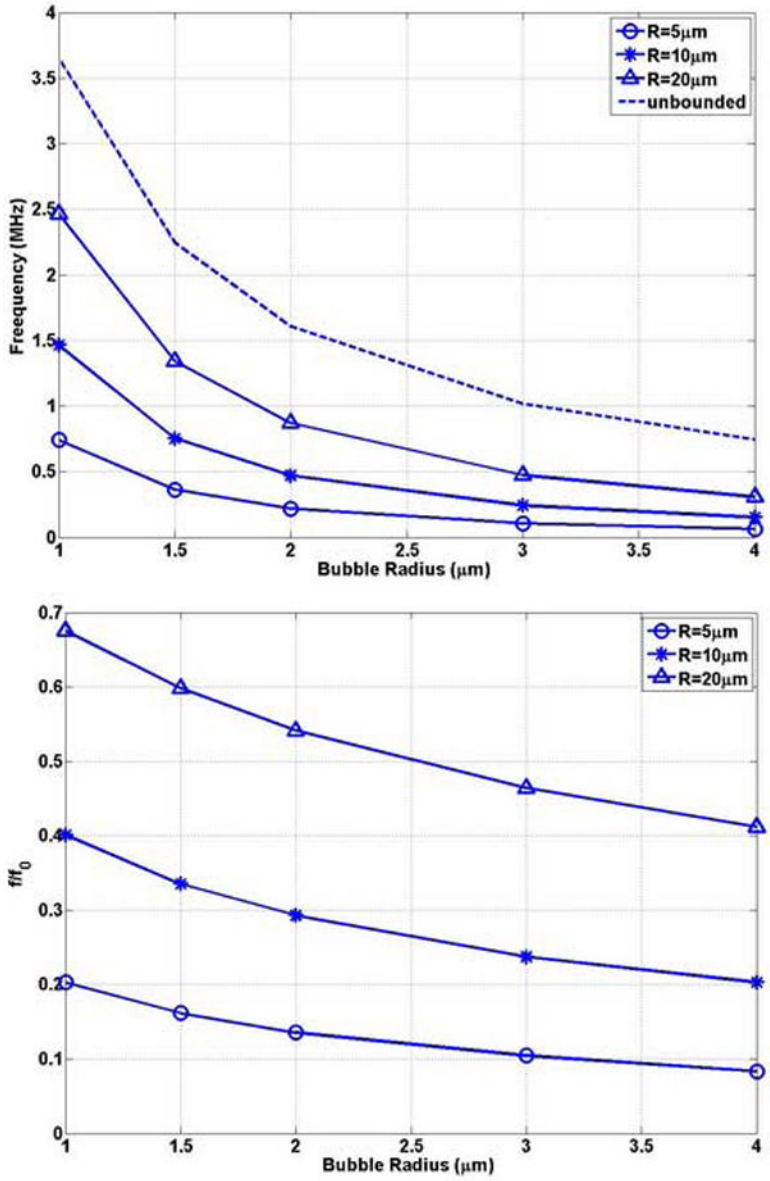

Figure 4.
The bubble natural frequency as a function of bubble radius for bubbles lying in the center of rigid vessels with $L = 500\mu m$: (a) dimensional natural frequency; (b) dimensionless natural frequency.

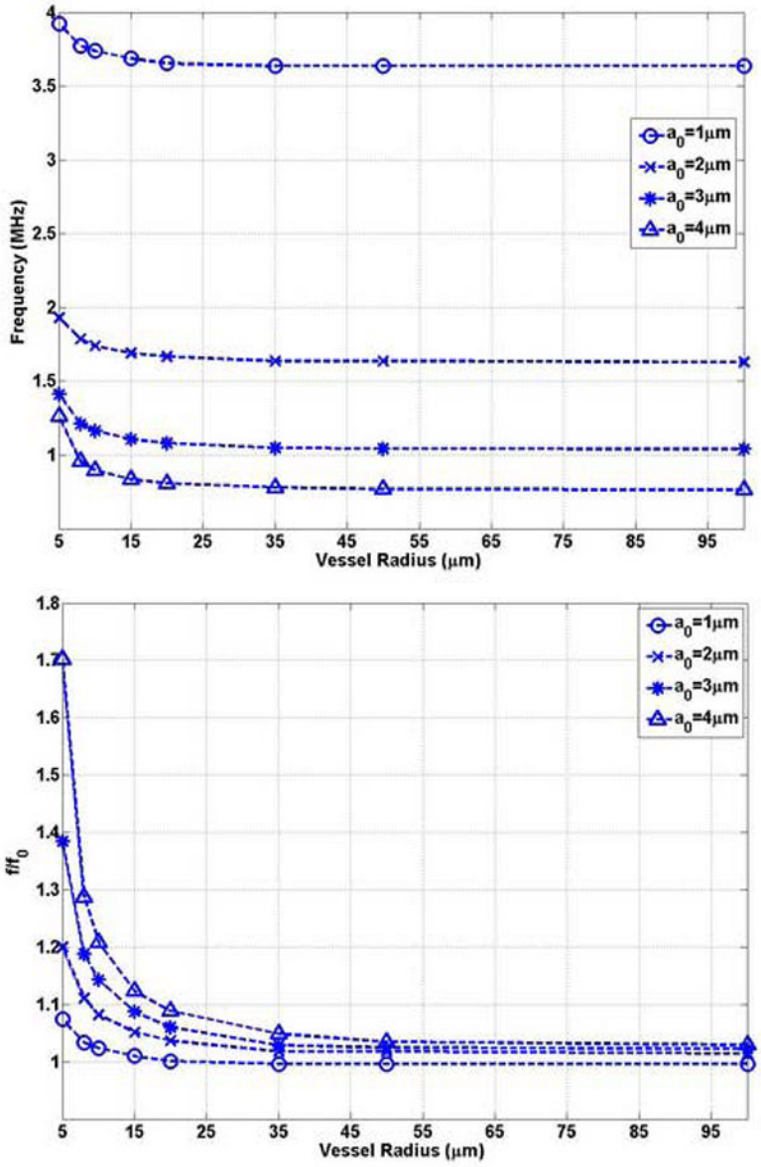

Figure 5.
The bubble natural frequency as a function of the vessel inner radius for bubbles lying in the center of compliable vessels with $L = 100\mu m$: (a) dimensional natural frequency; (b) dimensionless natural frequency.

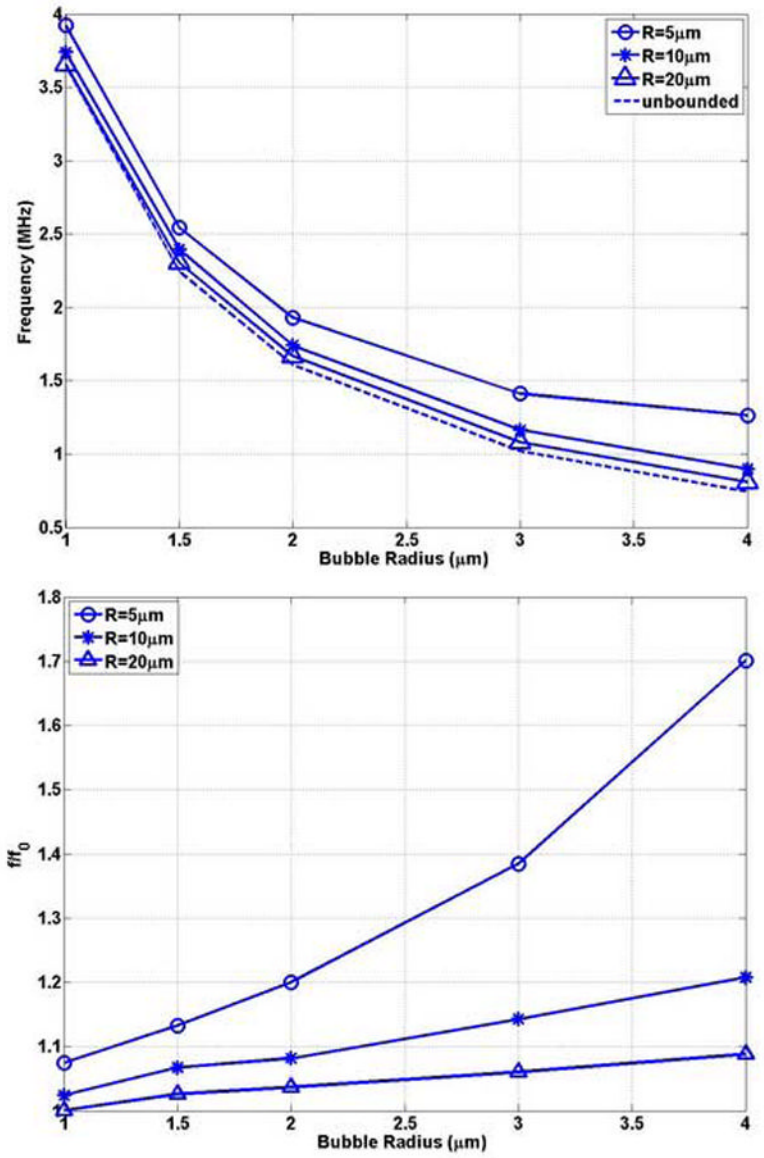

Figure 6.
The bubble natural frequency as a function of bubble radius for bubbles lying in the center of compliable vessels with $L = 100\mu m$: (a) dimensional natural frequency; (b) dimensionless natural frequency.

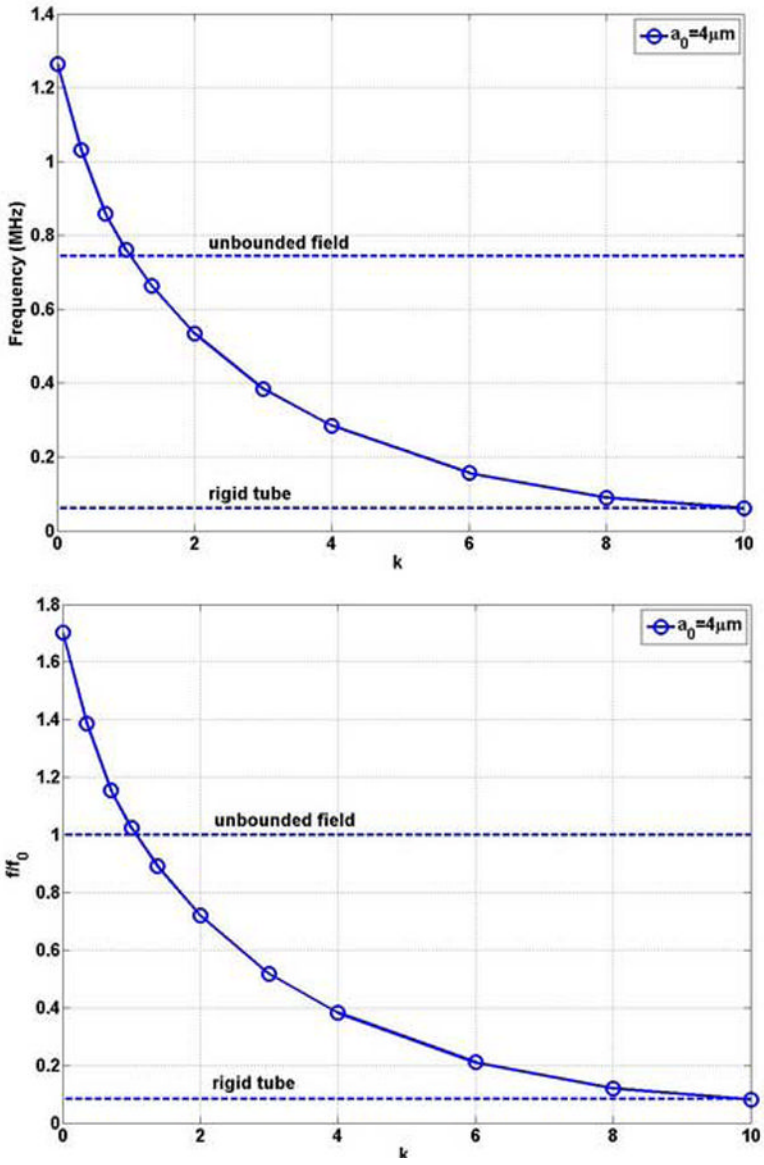

Figure 7.

The natural frequency of a bubble with $a_0 = 4\mu m$ as a function of the rigidity index k of the blood vessel in compliable vessel with R_0=5μm and $L = 500\mu m$ (a) dimensional natural frequency; (b) dimensionless natural frequency.

Table 1

Notation and values used(Sassaroli and Hynynen 2004; Sassaroli and Hynynen 2005)

Symbol	Definition	Values
ρ	blood density	1090 kg/m^3
η	blood effective dynamic viscosity	$2\times10^{-3} N\cdot s / m^2$
ρ_c	density of capillary	900kg/m^3
ρ_t	density of surrounding tissue	900kg/m^3
p_0	the initial pressure in surrounding interstitial liquid	101325Pa
p_{i0}	the initial intraluminal pressure	105370Pa
κ	polytropic index of gas inside the microbubble	1.0
σ	surface tension coefficient	0 .0643N/m
v	Poisson's ratio of the surrounding connective tissue	0.5
ξ	the nondimensional surrounding connective tissue thickness coefficient	0.1
a_0	microbubble's initial radius	
R_0	microvessel's initial inner radius	
L	microvessel length	
(v_r, v_z)	liquid velocity in the r and z direction, respectively	
p_i	intraluminal liquid pressure	
p_a	perivascular liquid pressure	
p_g	gas pressure in the microbubble	
p_{ge}	the gas pressure in a reference state	
t	time	
V	the microbubble volume	
V_e	microbubble volume in a reference state	
(r,θ,z)	coordinates of the particles in microvessel at current configuration	
l	intersection curve between the air-liquid interface and r-z plane in Figure 1(a)	
R_m	the midwall radius of microvessel at reference configuration	
H	the thickness of microvessel at reference configuration	
R_m	the midwall radius of microvessel at current configuration	
r_i	the inner radius of microvessel at current configuration	
r_a	the outer radius of microvessel at current configuration	
R_i	the inner radius of microvessel at reference configuration	
h_c	the thickness of microvessel at current configuration	
h_t	The effective dynamic thickness of the surrounding connective tissue	
Y	the Young's modulus of the surrounding connective tissue	
R_a	perosteal radius of the microvessel in its undeformed state	
$E_\theta (R_a, t)$	Green strain θ component at the exterior surface of the microvessel	
k	the nondimensional tumor rigidity index	